Post-print version of the article published in:
Materials Science and Engineering: B 01/2014; 184:80-87.
DOI: 10.1016/j.mseb.2014.01.017

Characterization of thermal properties of CdZnMgSe mixed crystals by means photopyroelectric and infrared imaging techniques

K. Strzałkowski

Institute of Physics, Faculty of Physics, Astronomy and Informatics, Nicolaus Copernicus University, Grudziadzka 5, 87-100 Torun, Poland
E-mail: skaroll@fizyka.umk.pl, phone: 00486113222, mob. 0048692631318

Abstract

In this work a complete thermal characterization of $Cd_{1-x-y}Zn_xMg_xSe$ mixed crystals was carried out. Bulk semiconductors under investigation were grown from the melt by a high pressure modified Bridgman method for different x and y content. The photopyroelectric method in the back configuration (BPPE) and the infrared (IR) lock-in thermography have been applied to measure values of the thermal diffusivity. Thermal effusivity of the samples was obtained with the PPE technique in the front configuration (FPPE), coupled with a thickness (TWRC-thermal wave resonator cavity) scanning procedure. Measured thermal effusivity together with the thermal diffusivity allowed calculating the thermal conductivity of the investigated materials. For the calculation of the specific heat the densities of the samples were estimated from their weight and geometry. The effect of Mg/Zn content ratio on thermal properties of this quaternary CdZnMgSe compounds was analyzed and discussed.

Keywords: A2B6; CdZnMgSe crystals; Lock-in Thermography; PPE method; Thermal properties.

1 Introduction

II-VI semiconductors are very promising materials from the point of view of application in construction of visible radiation sources in green laser diodes, spintronics, photodetectors and other applications in modern optoelectronics [1-3]. It is very important from the application point of view, that ternary and quaternary II-VI compounds allow almost smooth change of the band gap and lattice constant values [4]. CdZnMgSe semiconductor alloys are an interesting material for potential applications in ultraviolet to visible range emitters [5,6], infrared IR photodetectors [7], distributed Bragg reflectors [8,9] and mid-IR quantum cascade emitters [10,11]. The knowledge of the basic thermal properties of these solid solutions is important for proper device applications. Thermal parameters are unique for each material, strongly dependent on the composition, structural characteristic of the sample and the fabrication process. Quaternary CdZnMgSe compound can be treated as the mixture of CdSe, ZnSe and MgSe binary semiconductors as well as ternary CdMgSe and ZnMgSe crystals. Consequently, thermal properties of such an alloy exhibit a non-linear dependence of individual components. The aim of this article is performing complete thermal characterization (measurement of all static and dynamic thermal parameters) of the investigated materials and discuss the influence of the composition on their thermal properties.
Several experimental techniques were applied in order to achieve the objectives of this paper. Photopyroelectric methods have been extensively applied to the study of thermal properties of

condensed matter samples [12,13]. The major advantages of these techniques are their simplicity, high sensitivity, non-destructive character and adaptation on experimental restrictions for theoretical requirements. The thermal effusivity can be obtained in the front configuration (an incident radiation directly illuminates the sensor) coupled with TWRC method. In this technique, between the detector and the solid sample a coupling liquid is inserted, which is then being compressed. The main advantage of this configuration, compared to the classical frequency scanning methods, is connected with the possibility of controlling the type and the thickness of the coupling fluid. In principle, using this configuration, it is possible to obtain the thermal parameters of any layer in the system (if the others layers are known), but in this paper we will focus only on the thermal effusivity of the sample of interest, inserted as a backing material.
The PPE method in the back configuration (the sample placed onto the sensor is excited by an incident radiation) requires a thin layer of the coupling fluid between the sample and the pyroelectric sensor. In this work the thermal diffusivities measured with PPE technique were underestimated (5% lower) compared to those obtained with lock-in infrared thermography. This fact is in agreement with results obtained by Salazar and Oleaga [14-16]. They have shown that the results obtained with BPPE technique are always underestimated due to the presence of the coupling fluid between the sample and the sensor. The influence of the coupling fluid in pyroelectric measurements of solids becomes significant especially for high conductive samples and at high modulation frequency of incident radiation. One of the solutions to overcome this undesired effect could be a non-contact technique as infrared lock-in thermography.

2 Material and methods

Quaternary CdZnMgSe crystals were grown from the melt by the high-pressure, high-temperature modified Bridgman method using high purity powders of CdSe, ZnSe (99.995%), metallic Mg (99%) and Se (99.9%) put in a graphite crucible in stoichiometric proportion. This method allows obtaining crystal rods of about one centimeter in diameter and up to few in length. To remove processing dirt crystal rods were etched in hydrochloric acid and next cut perpendicular to the growth axis into about 1.4 mm thick samples. The plates were mechanically ground and then polished with diamond paste (1 μm). Their thickness and diameter were measured with a micrometer device (accuracy 10 μm). After the preparation samples were weighed with a Discovery OHAUS laboratory balance with a resolution 0.1 mg.
An experimental setup for the BPPE measurement [17] consisted of a green, current-modulated DPSS laser (532 nm) with the power of about 50 mW, a $LiTaO_3$ detector of the thickness 0.54 mm with Cr+Au electrodes and a SR830 lock-in processing the measured signal. In this configuration the sample is placed onto the sensor and is directly exciting by the incident radiation. A thin layer of ethylene glycol served as a coupling fluid between the sample and the sensor. To protect the detector from scattered light a black diaphragm was used. Frequency scans were performed in the range 0.3 Hz up to 15 Hz with 0.3 Hz single step. A blackening procedure with a thin carbon layer (< 10 μm) was applied to the samples in order (i) to assure the optical opacity of the transparent samples and (ii) to avoid the influence of an optical exciting state of the semiconductor on its thermal properties (phonon scattering processes on free excited carriers).
The front configuration (FPPE) coupled with the thickness scanning procedure consisted of a red He-Ne laser (Melles Griot, 30 mW) modulated with an acousto-optical modulator, a 215 μm thick LiTaO3 sensor coated with Cr+Au and a SR830 lock-in [18]. In this method the laser directly illuminates the sensor. The measured sample was put into the cell as a backing material. Between the sample and the sensor as coupling liquid with known thermal properties an ethylene glycol was inserted with the starting thickness of about 0.5 mm. The liquid was then compressed. Scanning procedure was performed by a 9062M-XYZ-PPP Gothic-Arch-Bearing Picomotor with a single step of 6 μm. The control of the parallelism between the backing and the sensor were assured by two 3 and 6-axis micrometric stages.

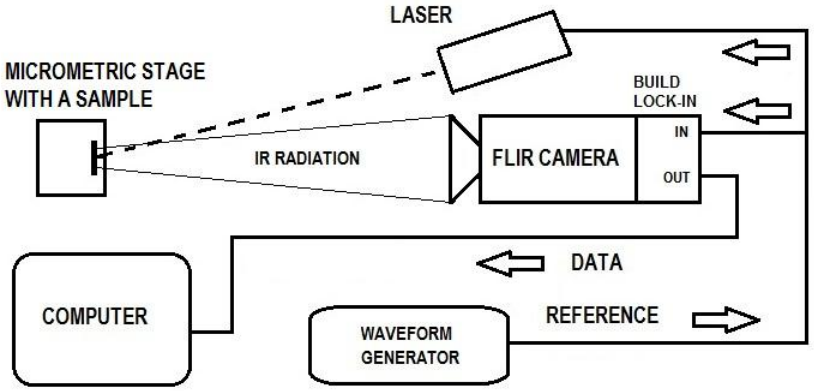

Fig. 1 Experimental setup for the lock-in thermography technique.

The experimental IR setup included a heat source, a waveform generator, an infrared camera and a computer for data acquisition (Fig. 1). The thermal images were collected from the blackened samples placed on a stage and excited with a green DPSS current-modulated laser (532 nm, 500 mW). The IR camera (FLIR 7200 Series) equipped with a 320x256 pixels array of InSb detectors with the spectral response in the range of wavelengths from 1.5 μm up to 5 μm recorded the changes in the surface temperature of the specimens. The noise equivalent temperature difference (NETD) of this camera is lower than 20 mK. The signals delivered by the infrared camera and the reference frequency f_0 were sent to the lock-in detection module incorporated into the camera, which outputs the continuous component image (f=0) as well as the amplitude and phase images of the f-component to a PC. The optical axis of the camera was perpendicular to the investigated surface. A glassy carbon (GC) type G with known thermal parameters (similar to the investigated crystals) was used as a reference sample [19]. All measurements presented in this paper were computer-controlled and performed at room temperature.

3 Theory

In a BPPE four-layer system a blackened sample *s* is placed on a pyroelectric sensor *p* and the whole system is surrounded by air (front and backing layers are air). Due to the fact that the blackening carbon layer is very thin (<10μm) and thermally very conductive one can neglect its influence on the signal. Assuming a perfect sample-sensor thermal contact and a one-dimensional model of the heat propagation through the sandwiched system, the complex PPE signal is given by [20,21]:

$$V = \frac{2V_0 e^{-\sigma_s L_s}}{b_{sp}+1} \frac{1-e^{-2\sigma_p L_p}}{1+R_{sp}e^{-2\sigma_p L_p}-(R_{sp}+e^{-2\sigma_p L_p})e^{-2\sigma_s L_s}} \qquad (1)$$

In Equation (1) V_0 is an instrumental factor, *ij* represents *s* and *p* layers of the detection cell, respectively, $R_{ij} = (b_{ij}-1)/(b_{ij}+1)$ is the reflection coefficient of the thermal wave at *ij* interface, $b_{ij} = e_i/e_j$ and *e* is thermal effusivity, $\sigma_i = (1+i)a_i$ is the complex diffusion coefficient, where a_i is the reciprocal of the thermal diffusion length μ_i, $a_i = 1/\mu_i$, $\mu_i = (2\alpha_i/\omega)^{1/2}$, ω is the angular modulation frequency and L_i is the thickness of the layer *i*. In order to eliminate the instrumental factor V_0 a normalization procedure must be performed (the signal is normalized with the signal obtained with empty sensor) [18]. After normalization, assuming thermally thick regime for both the detector and the sample ($\mu_i < L_i$), one can calculate the thermal diffusivity using the amplitude (Eq. 2) and/or the phase (Eq. 3), respectively [18]:

$$\ln|V_n| = \ln\frac{2}{b_{sp}+1} - a_s L_s \qquad (2)$$

$$\Theta = \Theta_0 - L_s\left(\frac{\omega}{2\alpha_s}\right)^{1/2} \quad (3)$$

In this paper we selected to calculate the thermal diffusivity from the slope of the curve $\Theta = \Theta(f^{1/2})$, after performing a frequency scan. The amplitude was not preferred because it can be often affected by external factors as long-term flow of the laser intensity.

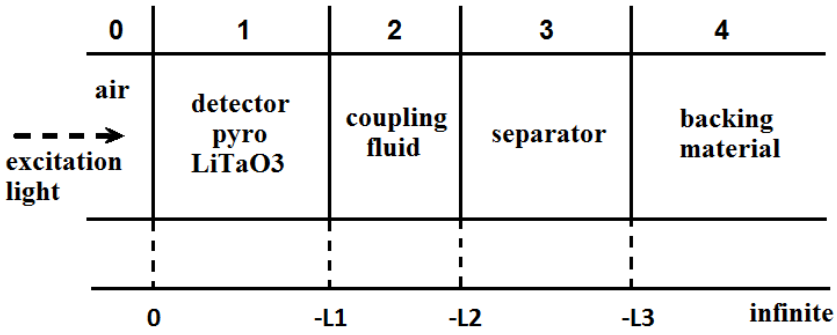

Fig. 2 The model of the cell in the front configuration for the TWRC method.

In the front configuration for TWRC method a general cell consisted of five layers (Fig. 2) was proposed [22]. In the approximation of a one-directional heat propagation the normalized complex PPE signal is given by:

$$V_n = \frac{1-R_{21}e^{-2\sigma_1 L_1}}{1-\rho_{21}e^{-2\sigma_1 L_1}}\frac{(e^{-\sigma_1 L_1}-1)-\rho_{21}(e^{-\sigma_1 L_1}-e^{-2\sigma_1 L_1})}{(e^{-\sigma_1 L_1}-1)-R_{21}(e^{-\sigma_1 L_1}-e^{-2\sigma_1 L_1})} \quad (4)$$

where:

$$R_{21} = \frac{1-b_{21}}{1+b_{21}}$$

$$\rho_{21} = \frac{(1-b_{21})+\rho_{32}(1+b_{21})e^{-2\sigma_2 L_2}}{(1+b_{21})+\rho_{32}(1-b_{21})e^{-2\sigma_2 L_2}}$$

$$\rho_{32} = \frac{(1-b_{32})+\rho_{43}(1+b_{32})e^{-2\sigma_3 L_3}}{(1+b_{32})+\rho_{43}(1-b_{32})e^{-2\sigma_3 L_3}}$$

$$\rho_{43} = \frac{1-b_{43}}{1+b_{43}}$$

If the backing material is air and in the same time L_3 is thermally thick ($\exp(-2\sigma_3 L_3) \sim 0$) ρ_{43} does not count and ρ_{32} is reduced to (a separator layer becomes the backing): $\rho_{32} = (1 - b_{32})/(1 + b_{32})$. The main advantage of this configuration, compared to the classical frequency scanning methods, is connected with the possibility of controlling the type and the thickness variation of the coupling fluid [18]. Moreover, no additional normalization measurement is required (according to Eq. 4); the normalization signal is contained in the same scanning run (thermally very thick regime for the scanned liquid). Basically, in this configuration, one can get the thermal parameters of each layer of the detection cell (if the thermal parameters of the other layers are known). In this paper we focused only on the thermal effusivity of the sample inserted as backing in the detection cell.

For infrared lock-in thermography a three dimensional model of heat propagation in the volume of the sample can be applied; however for the thermal diffusivity measurement only a surface temperature field is needed. In such a case the heat wave equation generated by a time-periodic

punctual heat source in an isotropic and homogeneous medium with thermal diffusivity α, can be written as:

$$\vec{T}(x,t) = T_o e^{j(2\pi ft - \vec{k}x)} \quad (5)$$

where x is the thermal wave propagation direction, T_0 is the surface temperature, f is the excitation frequency, t is the time and k is the wave vector. The 1-D thermal diffusion equation is given by:

$$\alpha \frac{\partial^2 \vec{T}(x,t)}{\partial x^2} = \frac{\partial \vec{T}(x,t)}{\partial t} \quad (6)$$

where:

$$\vec{k} = \pm(1-j)\sqrt{\frac{\pi f}{\alpha}} \quad (7)$$

For physical reasons, the thermal wave must converge at infinity, which requires:

$$\vec{k} = (1-j)\sqrt{\frac{\pi f}{\alpha}} \quad (8)$$

The thermal wave can be written as follows:

$$\vec{T}(x,t) = T_o e^{-\sqrt{\frac{\pi f}{\alpha}}x} e^{j\left(2\pi ft - \sqrt{\frac{\pi f}{\alpha}}x\right)} \quad (9)$$

The propagation of a plane thermal wave through a medium of the thickness x and the thermal diffusivity α, trains a phase shift $\Delta\varphi$ having the following expression:

$$\Delta\varphi = -\sqrt{\frac{\pi f}{\alpha}}x = px \quad (10)$$

where p is the slope of the phase-distance graph. The thermal diffusion length is expressed by:

$$\mu = \frac{1}{p} = \sqrt{\frac{\alpha}{\pi f}} \quad (11)$$

The thermal diffusivity can be written according to Eq. 11.

4 Results and discussion

Phase behavior of $Cd_{1-x-y}Zn_xMg_xSe$ mixed crystals for different x and y content and the reference GC sample as a function of the square root of the modulation frequency are given in Fig. 3. Presented scans were performed in different frequency ranges according to the thickness and the thermal diffusivity of measured samples. For low frequency regime nonlinear behavior can be seen caused by thermally thin ($\mu > L$) the sample and/or the sensor. If we want to estimate a cut-off frequency (the frequency delimitating the thermally thin/thick regimes) for our sensor (L_p=0.54 mm, α_p=1.06·10^{-6} m^2·s^{-1}) it is of about 1.2 Hz. Starting from f=4 Hz, the sensor and all samples are thermally thick. Consequently, linear fits have been performed in the frequency range from 4 Hz up to 15 Hz, using the least square method. Thermal diffusivity of the specimens was calculated according to Eq. 3.

In Fig. 4 phase characteristics of selected ZnSe, $Zn_{0.8}Mg_{0.2}Se$ and $Cd_{0.5}Zn_{0.1}Mg_{0.4}Se$ samples measured at 3 and 5 Hz respectively as the function of the liquid's thickness can be found. According to the theory two frequencies 3 Hz and 5 Hz were chosen so the backing sample is thermally thick and the sensor is still thermally thin. During the thickness scanning procedure thermal character of the liquid layer is changing from thermally thick to the thin one. For thermally thick regime the phase remains constant (it is used for the normalization) and goes to the minimum when the liquid becomes thermally thin. After the minimum is reached the phase increases very rapidly to its maximum. The higher value of the thermal effusivity of the backing wider and deeper minimum is observed as well as the difference between the minimum and maximum values in phase is increasing.

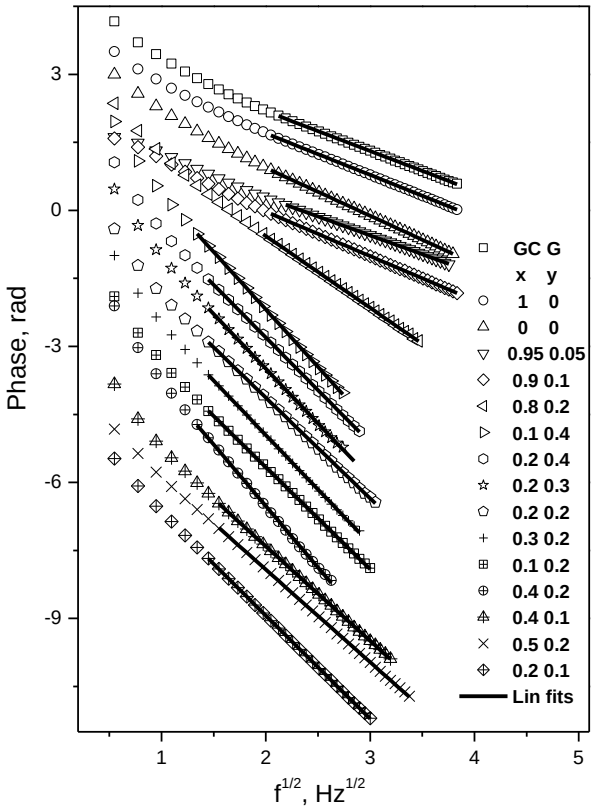

Fig. 3 Phase characteristics of $Cd_{1-x-y}Zn_xMg_xSe$ mixed crystals as a function of the square root of the modulation frequency, points are experimental data and lines are linear fits.

Consequently, ZnSe crystal got the highest value of the thermal effusivity in contrast to $Cd_{0.5}Zn_{0.1}Mg_{0.4}Se$ compound. In order to obtain the sample's thermal effusivity, numerical calculations have been performed, according to Eq. 4 with two fitting parameters: the effusivity of the backing material (sample) and the value of the absolute thickness of the fluid (distance between the sample and the sensor). The least square method was applied for the fitting procedure. The best theoretical fits are also displayed in Fig. 4.

For the thermal diffusivity measurements infrared imaging with a fast FLIR camera was introduced. Thermal images of selected ZnSe, $Zn_{0.8}Mg_{0.2}Se$ and $Cd_{0.5}Zn_{0.1}Mg_{0.4}Se$ samples obtained with the infrared lock-in thermography and corresponding phase profiles are presented in Fig. 5. Measurements were carried out in the frequency range 0.5 Hz up to 2 Hz so the samples under investigation were thermally thick. In presented thermal images imperfections caused by the presence of the blackening layer and the surface quality of the samples can be seen. The constant part of the phase in the center of the profiles is connected with the spot of the exciting laser. The linear fits were obtained with the least square method. Thermal diffusivity of the specimens was calculated according to Eq. 11.

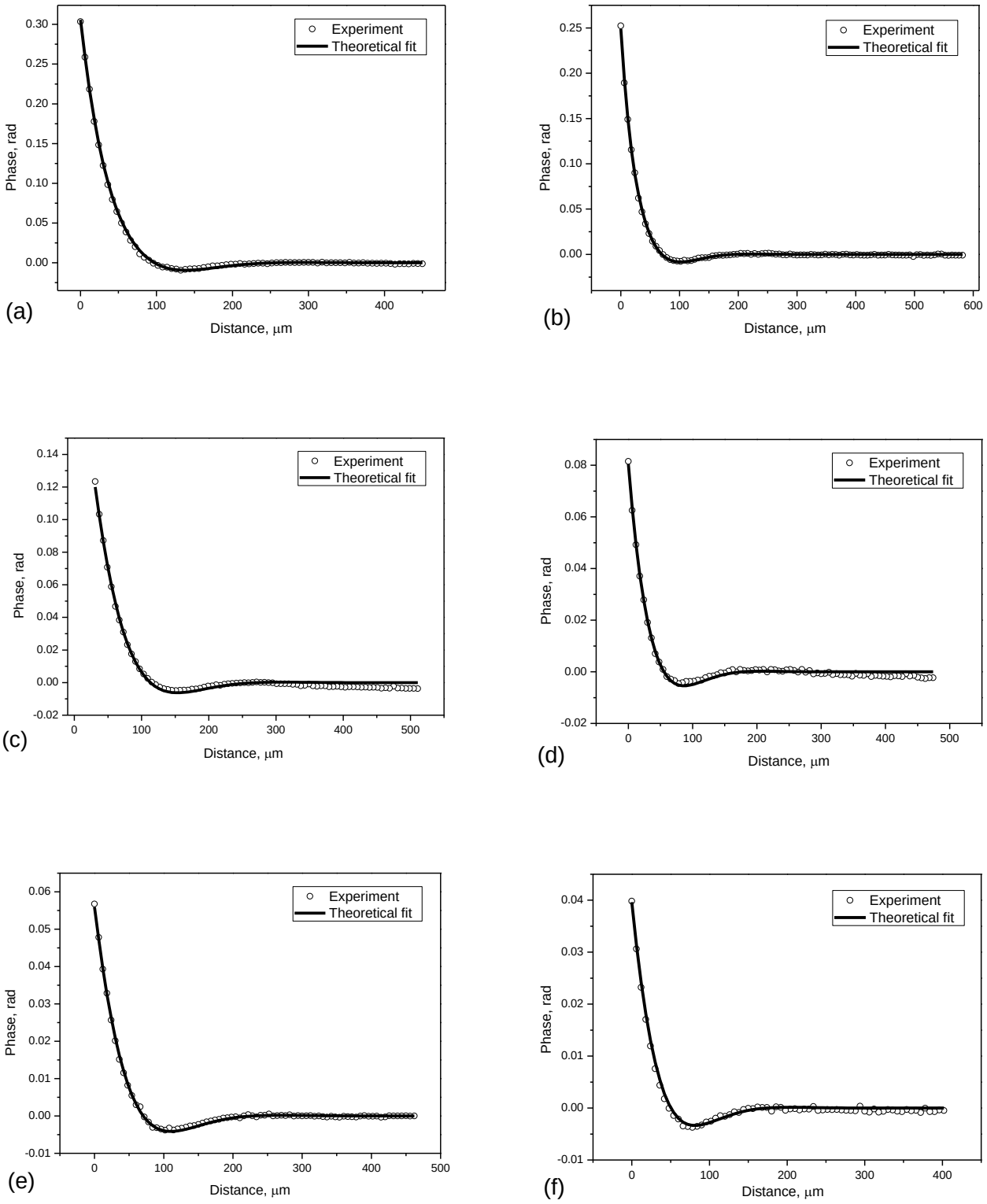

Fig. 4 Phase characteristics of ZnSe (a,b), $Zn_{0.8}Mg_{0.2}Se$ (c,d) and $Cd_{0.5}Zn_{0.1}Mg_{0.4}Se$ (e,f) samples measured at 3 (a,c,e) and 5 Hz (b,d,f) respectively with the thickness scan procedure in the front configuration, circles represent experimental results and lines are theoretical fits.

Table 1 Thermal parameters of the investigated $Cd_{1-x-y}Zn_xMg_ySe$ crystals and GC type G

x	y	Thermal cond. k ($W \cdot m^{-1} \cdot K^{-1}$)	Thermal diff. α ($m^2 \cdot s^{-1}$) $\cdot 10^{-6}$	Thermal effusivity ($W \cdot s^{1/2} \cdot m^{-2} \cdot K^{-1}$)	Specific heat ($J \cdot kg^{-1} \cdot K^{-1}$)	Density ($kg \cdot m^{-3}$)
1	0	13.3	6.3	5300	420.92	5016.51
0	0	4.53	3.5	2420	238.83	5400.8
0.95	0.05	8.96	4.51	4220	393.02	5056.05
0.9	0.1	6.35	3.17	3565	396.09	5055.12
0.8	0.2	3.27	1.9	2370	382.33	4497.13
0.1	0.4	1.49	0.99	1500	324.7	4646.78
0.2	0.4	1.71	1.03	1690	379.9	4387.16
0.2	0.3	1.46	1.04	1440	323.46	4375.93
0.2	0.2	1.63	1.04	1600	315.47	4969.27
0.3	0.2	1.76	1.06	1710	334.66	4966.88
0.1	0.2	1.94	1.10	1850	364.98	4832.92
0.4	0.2	1.88	1.14	1760	346.63	4765.97
0.4	0.1	2.00	1.18	1840	331.7	5103.01
0.5	0.2	2.08	1.19	1900	353.08	4926.06
0.2	0.1	1.83	1.26	1630	277.62	5223.63
GC type G		6.34	4.15	3110	1075.1	1420[a]

[a] Value taken from the literature for glassy carbon type G [19]

Thermal parameters of all measured samples are given in Table 1. The thermal diffusivity was estimated as the average of the results obtained from the PPE and the infrared lock-in thermography. It is to note that almost all values of the thermal diffusivity obtained with PPE were underestimated compared to the infrared camera ones; however the difference was within 5 %. This fact is well known and is in agreement with results obtained by other researchers. Salazar and Oleaga demonstrated [14-16] that results obtained from the BPPE are always underestimated because the coupler changes the slope of the curve $\Theta = \Theta(f^{1/2})$. The significance of the coupling fluid increases especially for high conductive samples and higher modulation frequencies. In this work, to overcome this undesired effect measurements were performed at low excitation frequencies, the coupling fluid was kept very thin and our samples are not high conductive materials. Additionally, each sample was measured three times and the obtained values of the thermal diffusivity were averaged.

In lock-in thermography the infrared camera measures the temperature of the specimen's surface. Blackening procedure applied to the samples can influence the results, especially for higher modulation of the incident radiation. In this work the modulation frequency was chosen as small as possible but the investigated samples were still kept in the thermally thick regime. This method is sensitive to the parallelism of the measured sample's surface to the detector of the camera because of possibility of measuring the projection of the temperature field. To minimize this effect for every sample two profiles have been taken from the thermal images and the thermal diffusivity was calculated as the average value from four slopes of the curves presented in Fig. 5 (b), (d) and (f), according to Eq. 11.

Thermal effusivities put in Table 1 were obtained from the FPPE technique as average values calculated from both applied frequencies. The difference of the thermal effusivities obtained for 3 and 5 Hz were up to 10 %. This can be explained due to imperfections of the surface of the backing material and nonparallel placement of the backing sample to the sensor.

Figure 6 presents contour maps of the precision of the fitings performed with Eq. 4 for ZnSe (a) and $Cd_{0.5}Zn_{0.1}Mg_{0.4}Se$ (b) samples respectively. The x and y axes represent the thermal effusivity of the backing material and the error in absolute value of the liquid layer, respectively. For ZnSe sample an effusivity ratio e_3/e_2 (backing/liquid) is about 6 and consequently, a good precision in the thickness but worse in the effusivity can be seen. On the other hand, for $Cd_{0.5}Zn_{0.1}Mg_{0.4}Se$ sample the ratio is two times smaller and thus reverse situation in the precision takes place.

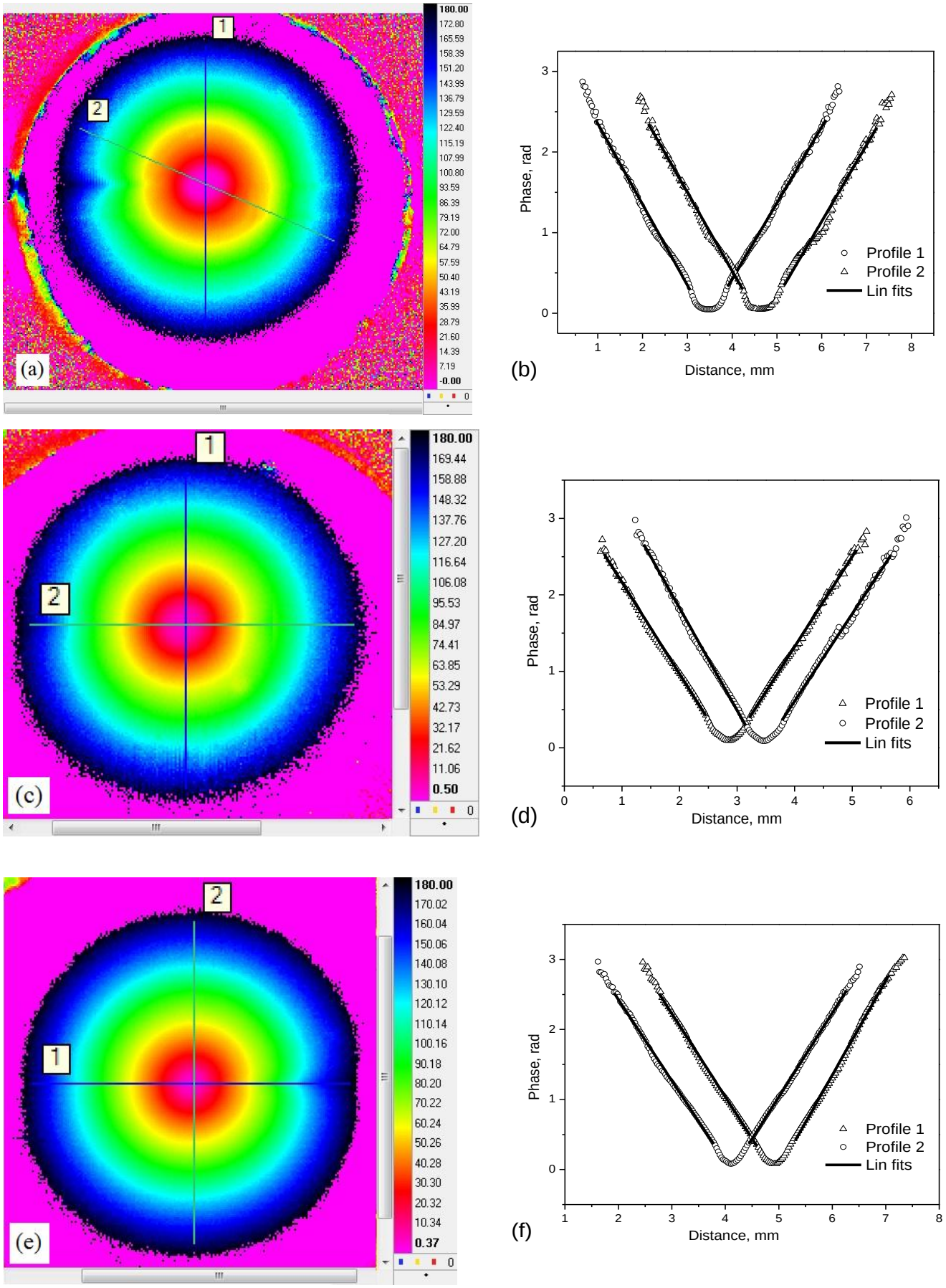

Fig. 5 Thermal images of the phase of the ZnSe (a), $Zn_{0.8}Mg_{0.2}Se$ (c) and $Cd_{0.5}Zn_{0.1}Mg_{0.4}Se$ (e) samples taken at 2, 1 and 0.5 Hz respectively and corresponding phase profiles (b,d,f) taken from the thermal images, circles correspond to measured data and lines are linear fits.

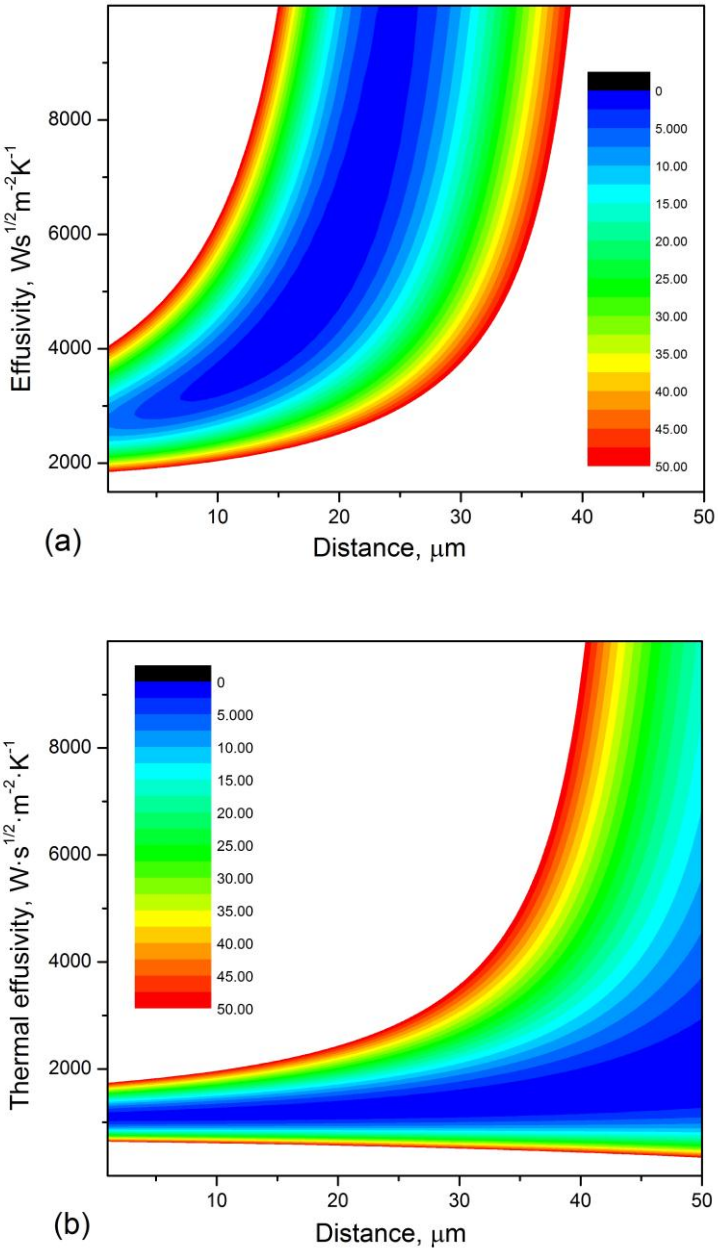

Fig. 6 Contour maps of the precision of the fitings performed with Eq. 2 for ZnSe (a) and $Cd_{0.5}Zn_{0.1}Mg_{0.4}Se$ (b) samples respectively.

The thermal diffusivity α and effusivity e for the density ρ and the specific heat C are connected by two relationships: $\alpha = k/(\rho C)$ and $e = (k\rho C)^{1/2}$, respectively. One can use them to calculate the thermal conductivity k from the formula: $k = e\alpha^{1/2}$. These three thermal parameters are not independent; to calculate the specific heat the density of the investigated samples were estimated from their weight and volume. The value of the thermal conductivity 6.34 $W \cdot m^{-1} \cdot K^{-1}$ obtained for the reference GC sample remains in very good agreement with the producer data (6.3 $W \cdot m^{-1} \cdot K^{-1}$), the difference is less than 1%. The specific heat of the glassy carbon was found by Pawlak et al. [17] from differential scanning calorimetry as 1050 $J \cdot kg^{-1} \cdot K^{-1}$ with the uncertainty of 2-5%. This value is in very good agreement with obtained in this work (1075.1 $J \cdot kg^{-1} \cdot K^{-1}$); the difference is less than 3%.

Obtained values of the thermal conductivities for ZnSe (x=1 and y=0) and CdSe (x=0 and y=0) crystals are smaller than literature [23] ones (19 and 9 $W \cdot m^{-1} \cdot K^{-1}$ respectively). It is well known

that thermal parameters strongly depend on the fabrication process, quality of the crystal structure, the defects and the concentration of the impurities. Considering binary ZnSe and CdSe crystals, all these, together with the non-ideal measurement conditions (assumption of one-dimensional heat propagation, presence of the blackening layer and coupling fluid) can explain the observed discrepancies between obtained values of thermal parameters and literature data.
In some sense the quaternary CdZnMgSe compound is the mixture of ZnSe, CdSe, MgSe, ZnMgSe and CdMgSe crystals and consequently, its thermal properties are resultant of all components.

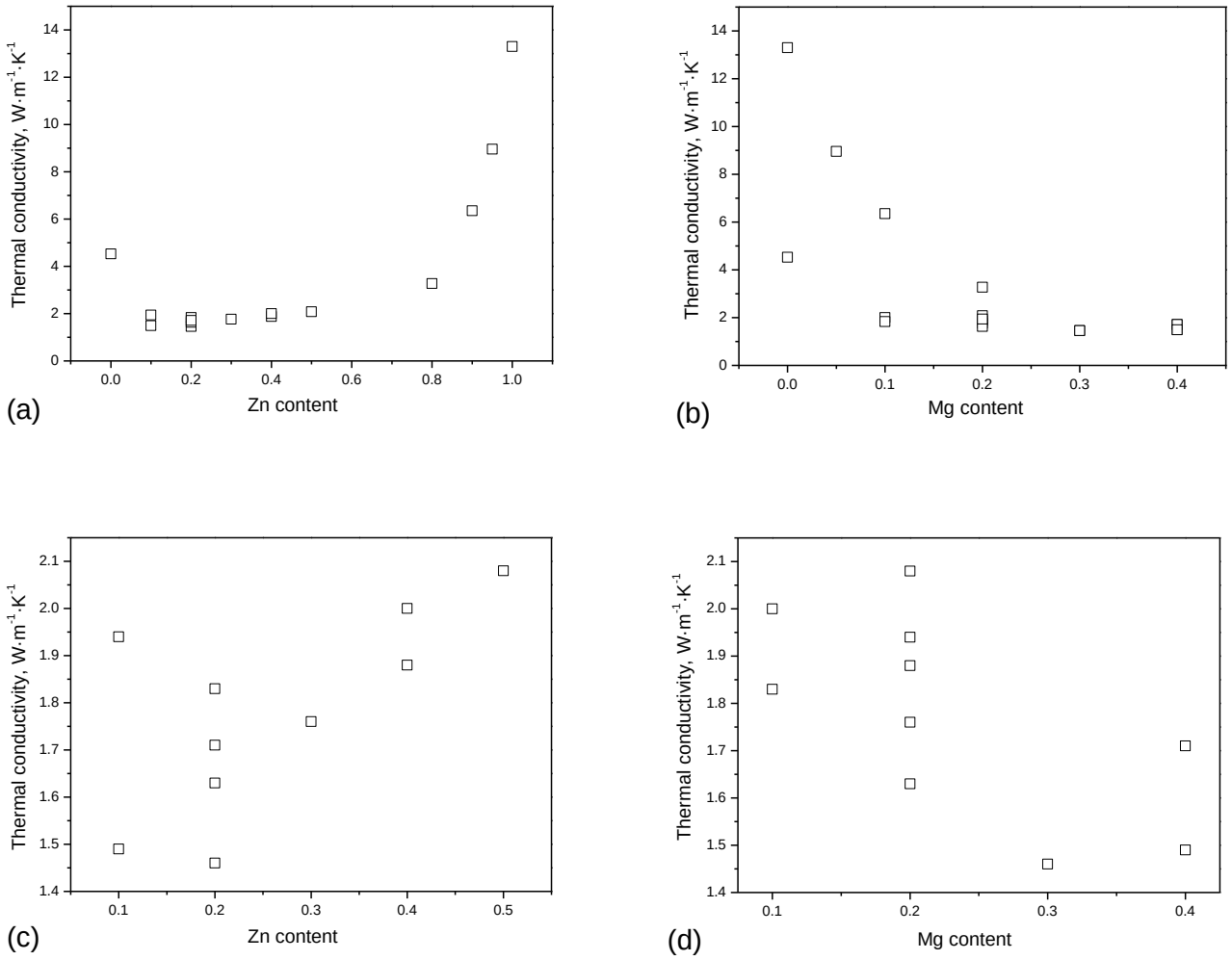

Fig. 7 Thermal conductivities of $Cd_{1-x-y}Zn_xMg_xSe$ crystals as a function of the composition, pictures (a) and (b) refer to all investigated crystals, pictures (c) and (d) presents results for quaternary CdZnMgSe compound.

Figure 7 presents thermal conductivities of all investigated crystals as a function of the composition. Pictures (a) and (b) in Fig. 7 refer to all investigated semiconductors, while pictures (c) and (d) present results only for quaternary CdZnMgSe compound. One can see the thermal conductivity is increasing with zinc content (a) while the crystals are approaching x=1 (highest conductivity ZnSe sample). On the other hand, adding magnesium lead to decreasing the thermal conductivity of the specimens (b). The same observation can be done for quaternary CdZnMgSe compounds on pictures (c) and (d), however in this case the difference in thermal conductivities are smaller and are up to 20%. Considering thermal diffusivity, similar effect was observed by Pawlak et al. [17] for CdMgSe crystals. One can conclude that adding magnesium to the CdZnMgSe alloy lead to increasing the concentration of crystal defects. In our opinion the main reason of this effect is the difference in atomic radius of the components and, as the consequence the periodic potential of the

crystal is perturbed. Every crystal imperfection in such a material may become a potential scattering center for phonons and consequently, the ability of the material to conduct the heat is reduced.

5 Conclusions

The samples under investigation were produced by high-pressure Bridgman method. In this paper the complete thermal characterization of the investigated $Cd_{1-x-y}Zn_xMg_ySe$ crystals was carried out using several different measurement techniques. The thermal diffusivity of the samples was obtained from the PPE method in the back measurement configuration and from the infrared imaging using FLIR camera with the lock-in detection. The values of the thermal effusivity were derived from the PPE technique in the front configuration coupled with the TWRC method. Two thermal parameters in a combination with calculated densities of the samples allowed calculating their thermal conductivity and specific heat values. The thermal parameters obtained for the reference GC sample are in good agreement with the literature data. On the other hand, the thermal conductivity of binary crystals was different than found in references. In case of the thermal properties the fabrication process, the quality of the crystal structure, defects and the concentration of the impurities play significant role. All assumptions, imperfections of the samples and non-ideal experimental conditions introduced some additional uncertainty. In case of CdZnMgSe alloys the thermal conductivity was very low, especially for high concentration of magnesium. The reason of producing such alloys is ability to change their structural and optical properties to the desired ones. However, in the same time the thermal properties of the material are getting worse what should be taken into account because of the problem of the heat dissipation in miniaturized optoelectronic devices.
In case of solid samples a coupling medium is often required; it always introduces some additional uncertainty to the system. One of the solutions could be infrared lock-in thermography, which in principle is free from this problem. A short comparison of pyroelectric and infrared imaging techniques leads to the conclusion that, from technical point of view, the IR thermography presents some clear advantages: it is faster and, being a noncontact technique, no coupling fluid is necessary.

Acknowledgements

The study was supported by research fellowship within project “Enhancing Educational Potential of Nicolaus Copernicus University in the Disciplines of Mathematical and Natural Sciences” (project no. POKL.04.01.01-00-081/10.).

References

[1] T. Nakamura, K. Katayama, H. Mori, S. Fujiwara, Novel cladding structure for ZnSe-based white LEDs with longer lifetime over 10,000 hours, Phys. Stat. Sol. B 241 (2004) 2659-2663.
[2] M. Adachi, K. Ando, T. Abe, N. Inoue, A. Urata, S. Tsutsumi, Y. Hashimoto, H. Kasada, K. Katayama, T. Nakamura, Slow-mode degradation mechanism and its control in new bright and long-lived ZnSe white LEDs, Phys. Stat. Sol. B 243 (2006) 943-949.
[3] Y. Niiyama and M. Watanabe, BeMgZnSe-based ultraviolet lasers, Semicond. Sci. Technol. 20 (2005) 1187-1197.
[4] F. Rozpłoch, J. Patyk, F. Firszt, S. Łęgowski, H. Męczynska, J. Zakrzewski, A. Marasek, Raman, Photoluminescence and Photoacoustic Investigations of $Zn_{1-x-y}Be_xMn_ySe$ Mixed Crystals, Phys. Stat. Sol. B 229 (2002) 707-709.
[5] W. Lin, A. Cavus, L. Zeng, M. C. Tamargo, N-type doping of lattice-matched ZnCdSe and $Zn_xCd_yMg_{1-x-y}Se$ epilayers on InP using $ZnCl_2$, J. Appl. Phys. 84 (1998) 1472-1475.

[6] K. Kishino and I. Nomura, II-VI semiconductors on InP for green-yellow emitters, IEEE J. Sel. Top. Quantum Electron. 8 (2002) 773-786.
[7] H. Lu, A. Shen, M. C. Tamargo, C. Y. Song, H. C. Liu, S. K. Zhang, R. R. Alfano, M. Munoz, Midinfrared intersubband absorption in $Zn_xCd_{1-x}Se/Zn_xCd_yMg_{1-x-y}Se$ multiple quantum well structures, Appl. Phys. Lett. 89 (2006) 131903-131905.
[8] T. Morita, H. Shinbo, T. Nagano, I. Nomura, I. Kikuchi, K. Kishino, Refractive index measurements of MgZnCdSe II–VI compound semiconductors grown on InP substrates and fabrications of 500–600 nm range MgZnCdSe distributed Bragg reflectors, J. Appl. Phys. 81 (1997) 7575-7579.
[9] O. Maksimov, S. P. Guo, L. Zeng, M. C. Tamargo, F. C. Peiris, J. K. Furdyna, Distributed Bragg reflectors based on (Zn,Cd,Mg)Se for use in the visible spectral range, J. Appl. Phys. 89 (2001) 2202-2207.
[10] W. O. Charles, A. Shen, K. J. Franz, C. Gmachl, Q. Zhang, Y. Gong, G. F. Neumark, M. C. Tamargo, Growth and characterization of $Zn_xCd_{1-x}Se/Zn_xCd_yMg_{1-x-y}Se$ asymmetric coupled quantum well structures for quantum cascade laser applications, J. Vac. Sci. Technol. B 26 (2008) 1171-1173.
[11] W. O. Charles, Y. Yao, K. J. Franz, Q. Zhang, A. Shen, C. Gmachl, M.C. Tamargo, Growth of Znx,Cd(1−x)Se/ZnxCdyMg(1−x−y)Se–InP quantum cascade structures for emission in the 3–5 μm range, J. Vac. Sci. Technol. B 28 (2010) C3G24-C3G27.
[12] H. Coufal and A. Mandelis, Pyroelectric sensors for the photothermal analysis of condensed phases, Ferroelectrics 118 (1991) 379-409.
[13] D. Dadarlat, M. Chirtoc, R. Candea, I. Bratu, Direct pyroelectric detection of optical absorption in non-transparent materials, Infrared Phys. 24 (1984) 469-471.
[14] A. Salazar, On the influence of the coupling fluid in photopyroelectric measurements, Rev. Sci. Instrum. 74 (2003) 825-827.
[15] A. Salazar and A. Oleaga, A New Method to Overcome the Underestimation of the Thermal Diffusivity of Solid Samples Induced by the Coupling Fluid in Photopyroelectric Measurements, Int. J. Thermophys. 33 (2012) 1901-1907.
[16] A. Salazar and Oleaga, Overcoming the influence of the coupling fluid in photopyroelectric measurements of solid samples, Rev. Sci. Instrum. 83 (2012) 014903-014907.
[17] M. Pawlak, F. Firszt, S. Łęgowski, H. Męczyńska, J. Gibkes, J. Pelzl, Thermal Transport Properties of Cd1−xMgxSe Mixed Crystals Measured by Means of the Photopyroelectric Method, Int. J. Thermophys. 31 (2010) 187-198.
[18] D. Dadarlat, Photopyroelectric calorimetry of liquids; recent development and applications, Laser Phys. 19 (2009) 1330-1339.
[19] http://www.htw-gmbh.de/, August 2013.
[20] M. Chirtoc and G. Mihailescu, Theory of the photopyroelectric method for investigation of optical and thermal materials properties, Phys. Rev. B 40 (1989) 9606-9617.
[21] A. Mandelis and M.M. Zver, Theory of photopyroelectric spectroscopy of solids, J. Appl. Phys. 57 (1985) 4421-4430.
[22] J. Shen and A. Mandelis, Thermal wave resonator cavity, Rev. Sci. Instrum. 66 (1995) 4999-5005.
[23] O. Madelung, Semiconductors: Data Handbook, Springer-Verlag, Germany, 2003.